

THE STRUCTURE OF NGC 1976 IN THE RADIO RANGE

T. L. WILSON¹, S. CASASSUS², AND KATIE M. KEATING³

¹ US Naval Research Laboratory, Code 7210, Washington, DC 20375, USA; tom.wilson@nrl.navy.mil

² Departamento de Astronomia, Universidad de Chile, Casilla 36-D, Santiago, Chile

³ National Research Council Postdoctoral Research Associate, US Naval Research Laboratory, Code 7213, Washington, DC 20375, USA

Received 2011 October 6; accepted 2011 November 22; published 2011 December 22

ABSTRACT

High angular resolution radio continuum images of NGC 1976 (M42, Orion A) at $\nu = 330$ MHz ($\lambda = 91$ cm), 1.5 GHz (20 cm), and 10.6 GHz (2.8 cm) have been aligned, placed on a common grid, smoothed to common resolutions of $80''$ ($=0.16$ pc at 420 pc) and $90''$ ($=0.18$ pc) and compared on a position-by-position basis. The results are *not* consistent with a single value of T_e . The best fit to the continuum data is a multi-layer model based on radio recombination line data with a monotonic variation, from $T_e = 8500$ K in the higher intensity, more compact region at the rear of NGC 1976 to $T_e = 6000$ K in the low-intensity, extended region in the foreground. An estimate of temperature fluctuations toward the peak from this model yields $t^2 = 0.003$. This is a factor of 10 lower than fluctuation values from optical collisionally excited line data.

Key words: H II regions – ISM: individual objects (NGC 1976, M42, Orion A) – radio continuum: ISM – radio lines: ISM

Online-only material: color figures

1. INTRODUCTION

The H II region NGC 1976 (or M42, Orion A) is the most studied such source in our galaxy. At a distance of 420 pc (the average obtained from Sandstrom et al. 2007, Menten et al. 2007, and Hirota et al. 2007), this is the nearest site of high-mass star formation. The H II region itself has been studied extensively in the infrared, radio, and optical ranges (see, e.g., O’Dell 2001, 2003). Behind and in contact with NGC 1976 is the much more massive Orion molecular cloud. The molecular cloud remains stationary while NGC 1976 is a very thin region expanding toward the Sun (see, e.g., O’Dell 2003) with a boundary traced by molecular fragments such as CN (Rodriguez-Franco et al. 2001). The H II region has been modeled using radio continuum and radio recombination line (hereafter RRL) data. The observable parameters of such models are the electron densities, N_e , electron temperatures, T_e , radial velocities V , turbulent linewidths, ΔV_{turb} , and ionization structure, averaged along the line of sight (LOS) and over the telescope beam. For models of NGC 1976, the geometry is a set of face-on cylindrical layers (Lockman & Brown 1975, hereafter LB; Shaver 1980; Wilson & Jaeger 1987). Then the LOS averages can be converted into a three-dimensional distribution to the limit set by the angular resolution. These models can be compared with data from infrared or optical wavelengths. Afflerbach et al. (1996, 1997) carried out measurements of IR lines, which were combined with radio data to directly estimate element abundances for sources in the inner galaxy. A full understanding of radio T_e determinations for a sample of nearby regions would aid interpretations for more distant sources.

2. MODELS BASED ON RRLs

The first internally consistent RRL model of an H II region was by Brocklehurst & Seaton (1972, hereafter BS). For the analysis of RRL emission, detailed radiative transfer is needed. This was first carried out by BS for a spherical geometry. Later LB, Shaver (1980), and Wilson & Jaeger (1987, hereafter WJ) refined the model by using a multi-layer, slab geometry. For NGC 1976,

a geometry where diameters are much larger than LOS depths is needed since the RRL data require local densities in excess of the rms average densities (see the Appendix). Most of the RRL data were taken toward the continuum maximum with a variety of angular resolutions. Decisive tests of these models require determinations of T_e from RRL maps. In this face-on slab geometry, the more extended parts of the nebula are closer to the Sun. The model of LB predicted a rise in T_e in the more extended parts of NGC 1976 compared to the rear, while the Shaver (1980) model is isothermal. The data taken by WJ showed that the value of T_e is lower further from the center of NGC 1976. These results led to the WJ model in which the most extended, lower density layer is closer to the observer, with N_e and T_e increasing with increasing distance from the observer. The maximum value of T_e reached 8500 K for the compact dense gas at the interface to the background molecular cloud to the rear. The WJ model is consistent with the RRL data taken from 600 MHz to 100 GHz toward the source peak, and 22 GHz radio continuum scans in right ascension and declination, and maps in RRLs. Thus, this model is the starting point for an analysis of continuum images at frequencies of 330 MHz (Subrahmanyan et al. 2001; resolution $79'' \times 65''$) 1.5 GHz (Felli et al. 1993; resolution $28''$) and 10.6 GHz (Subrahmanyan et al. 2001; resolution $90''$).

The WJ model is based on the radiative transfer method of BS (in a radiative transfer computer code from C. M. Walmsley) and incorporates the face-on layered geometry introduced by LB and improved by Shaver (1980). A major change from earlier models was the introduction of a decrease in T_e from back to front of the source. This was based on the measurement of T_e at four positions $4'$ from the peak in the hydrogen 110α line ($\nu = 4.87$ GHz) and $H139\beta$ ($\nu = 4.79$ GHz). At these positions, non-LTE effects are expected to be negligible since the continuum intensities at 4.8 GHz are small, so τ is <0.05 (see Equations (A2) and (A3)). From these data, the derived T_e values away from the continuum peak are smaller than toward the peak. These data are consistent with a monotonic decline of T_e for positions away from the peak. In the layer geometry, this is interpreted as a decline in T_e from the back of the source to the foreground outermost layer. This fall-off in T_e was an important

difference between the models of WJ, LB, and Shaver (1980). The WJ model was originally a five-layer face-on slab geometry. To better fit continuum images, the four innermost layers were divided into two parts, each with one-half the LOS depth, the same N_e and T_e , and the layer nearer the Sun having a larger extent perpendicular to the LOS. The outermost layer, closest to the Sun, was left single. Thus the five-layer model grew to nine layers. As shown by WJ, the RRL data toward the peak could be fit using the LB, Shaver (1980), or WJ models, so only results from RRL mapping data allowed a decision between these.

3. RADIO CONTINUUM DATA

In principle, T_e can be determined from radio continuum data. The relation for a single isothermal region in the Rayleigh–Jeans regime is (see, e.g., Wilson et al. 2009):

$$T_B = T_e(1 - e^{-\tau_{ff}}), \quad (1)$$

where τ_{ff} is the free–free optical depth (see the Appendix for a discussion of τ_{ff}). T_B is the true brightness temperature. This becomes the main beam brightness temperature if the source is much larger than the telescope beam.

A number of methods have been used to estimate values of T_e . The first is to solve Equation (1) for the case when $\tau \gg 1$. For NGC 1976, this requires measurements at a low frequency. For a discrete source, the value of T_B is not directly measured, but this can be obtained from measurements of the peak intensity as main beam brightness temperature, T_{MB} , accurate calibrations, and measurements of the beam and source size. The usual assumption is that the beam and source have Gaussian shapes. From single telescope data, the core of NGC 1976 has a rather large intensity and an angular size of ~ 2.5 , but there is lower intensity emission from the nebula over a total extent of $\sim 30'$ (see, e.g., Wilson et al. 1997; Dicker et al. 2009). From the variation of flux density with frequency, the value of τ_{ff} of the core of NGC 1976 is larger than unity below 1 GHz, so from Equation (1), high angular resolution measurements for frequencies below 1 GHz can provide a good determination of T_e . Mills & Shaver (1968) reported a value of $T_e = 7600 \pm 800$ K using a 3.2 beam at 408 MHz. Subrahmanyan et al. (2001) measured a peak value of 3.84 Jy with a $65'' \times 79''$ beam at 330 MHz using the Very Large Array (VLA). This yields a peak temperature of $T_{MB} = 8400$ K. The optical depth of the source is large and the source is extended, so this is close to the value of T_e . We estimate that the error from noise is less than 30 K. Felli et al. (1993) measured a peak intensity of 6.3 Jy with a $28''$ beam at 1.5 GHz, using the VLA in the C and D configurations. This yields a peak temperature of $T_{MB} = 4600$ K. We estimate that the error from noise is less than 12 K. However at 1.5 GHz, the optical depth of Orion is below unity, so the value of T_e is rather uncertain (Equation (1)).

A second method consists of determining T_e and τ_{ff} from a fit to the source flux density as a function of frequency. This fit is based on an application of Equations (1), (A3), and (A5). In addition, there must be a number of measurements over a wide range of frequencies (see, e.g., Terzian & Parrish 1970). The errors in such determinations are often underestimated since the zero levels, limits of integration to determine the total flux density and calibrations may be inaccurately determined. A smaller effect is that the flux density of the nearby source NGC 1977 must be separated from the total integrated flux density.

A third method was presented by Dicker et al. (2009). These authors introduced a more elaborate approach. In this,

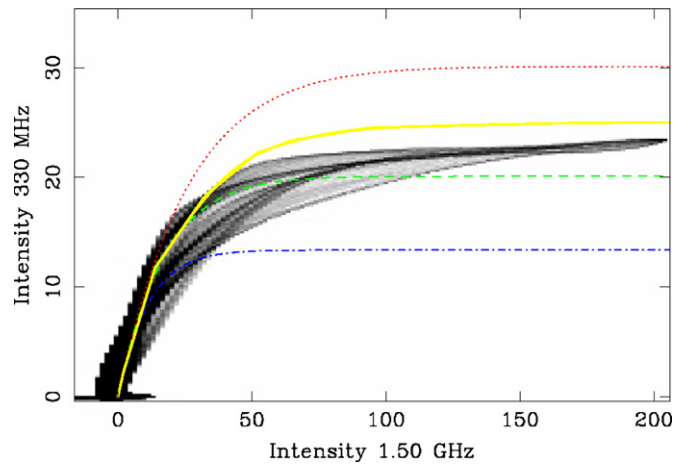


Figure 1. Plot of the relationship between radio continuum intensities for a pair of frequencies. Rather than using a scatter plot, which gives rise to crowded regions and deemphasizes outliers, we have plotted the data as a grayscale representation. The units are MJy per sr. The 330 MHz data are from Subrahmanyan et al. (2001) and 1.5 GHz (Felli et al. 1993). Both data sets were smoothed to $80''$ resolution, with maxima aligned and data placed on the same grid points. This plot follows the method of Dicker et al. (2009). The dotted line is for a model made following Equation (1), smoothed to $80''$ resolution, with a constant electron temperature of $T_e = 9000$ K (shown in red), the dashed line is for a constant electron temperature of $T_e = 6000$ K (shown in green), the dash-dotted line is for a constant electron temperature of $T_e = 4000$ K (shown in blue). The thicker solid line is for the WJ model (parameters in that paper). (A color version of this figure is available in the online journal.)

T_e is determined using resolved, calibrated images taken at two frequencies. These are smoothed to a common resolution, aligned and placed on a common grid. Then, intensities are plotted on a position-by-position basis to determine unique values of T_e . The analysis does not depend on geometry or a knowledge of τ_{ff} . In Figure 1, we follow the scheme of Dicker et al. (2009), plotting the intensities for 330 MHz (data of Subrahmanyan et al. 2001) and 1.5 GHz (data of Felli et al. 1993). In our approach, we did not allow for a DC offset or intensity calibration error (as was done by Dicker et al. 2009). This offset would allow for zero point errors in the data, but adds to the number of free parameters. These DC offsets are significant in regard to the integrated flux densities, but are about 1 MJy sr^{-1} so are negligible compared to the specific intensities. The fit procedures of Dicker et al. (2009) resulted in offsets of a similar magnitude. From Figure 1 there is only a small scatter about the origin. Thus we dispensed with this degree of freedom. The data for both wavelengths were smoothed to $80''$, the maxima aligned and placed on a common grid. In addition, there are plots for isothermal models for $T_e = 4000$ K, 6000 K, and 9000 K. From these results, there is a systematic difference with respect to the models of constant T_e , so these data are *not* consistent with a single value of T_e . For lower intensities, the data agree with a T_e value of ~ 6000 K, while for higher intensities, the agreement is with a T_e value of ~ 8500 K. Given the averaging along the line of sight, it is difficult to deduce a model from this data, but one *can* test models on the basis of agreement with the data plotted in Figure 1.

The best choice is a comparison with the WJ model, since this agrees with RRL mapping data. From a by-eye comparison, the WJ model is more consistent than plots for a constant T_e . The agreement between model and data was improved by lowering the T_e values in the three outermost layers by 8%. A question is how this change will affect the RRL results. The RRL data for 5–25 GHz are of good quality, so tightly constrain T_e and N_e of

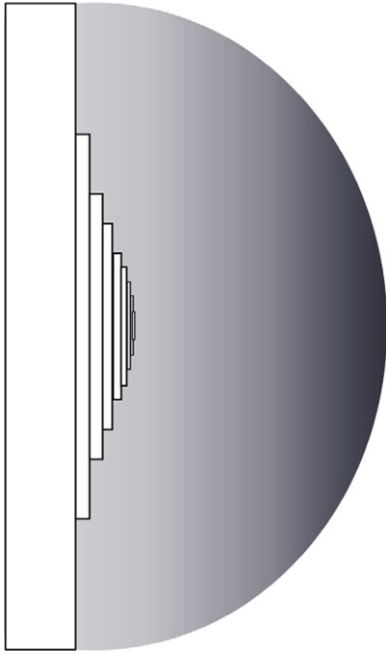


Figure 2. Side view of the model whose parameters are presented in Table 1. The shaded region to the right represents a part of the Orion Molecular Cloud. The observer is to the left side. Layer 9 of the Orion H II region is represented by the largest rectangle closest to the observer, layer 1 is the smallest rectangle, to the right. The relative sizes of the layers are to scale. The parameters of the layers are given in Table 1.

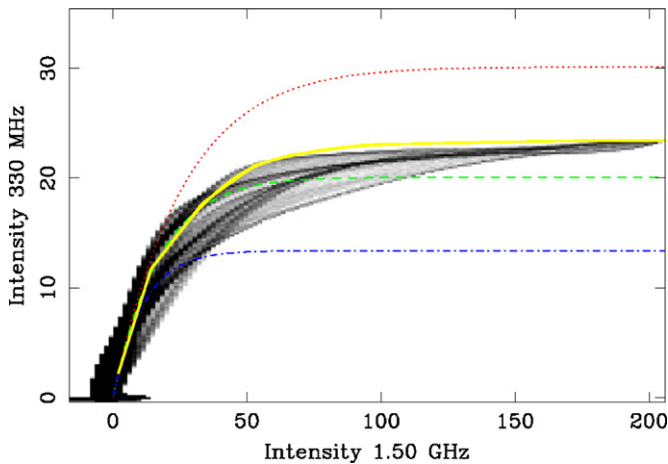


Figure 3. Data and constant T_e models are the same as in Figure 1. The improved WJ model is shown as a thicker yellow solid line (parameters in Table 1 and see Figure 2). The other lines are as in Figure 1, that is, with $T_e = 9000$ K (shown in red), the dashed line is for a constant electron temperature of $T_e = 6000$ K (shown in green), the dash-dotted line is for a constant electron temperature of $T_e = 4000$ K (shown in blue).

(A color version of this figure is available in the online journal.)

layers 1–6. Lowering the T_e for layers 7, 8, and 9 will not affect the parameters for layers 1–6 by more than 8%. The RRL data taken below 1 GHz mostly arise from layers 7, 8, and 9. At these lower frequencies, the RRL linewidths and to some extent the line intensities have larger measurement errors, so the model is less constrained by these results.

A side view of this model is given in Figure 2. This improved model is compared with data in Figure 3, where we show this model as a thicker solid line. In Figure 4, we plot intensity versus intensity for the 1.5 GHz and 10.6 GHz data. From this plot, the difference between the improved WJ and isothermal models is

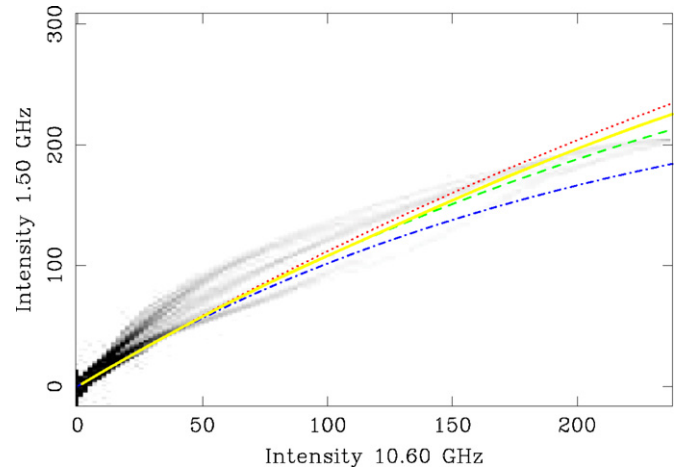


Figure 4. Data sets processed are the same as in Figure 1. Here the data were taken at 10.6 GHz (Subrahmanyam et al. 2001) and 1.5 GHz (Felli et al. 1993). Both data sets were smoothed to $90''$ resolution, with maxima aligned and data placed on the same grid points. The dashed, dotted, and dash-dotted lines are for constant temperature models as in Figure 1, that is, with $T_e = 9000$ K (shown in red), the dashed line is for a constant electron temperature of $T_e = 6000$ K (shown in green), the dash-dotted line is for a constant electron temperature of $T_e = 4000$ K (shown in blue). The thicker solid yellow line is the improved WJ model (Table 1).

(A color version of this figure is available in the online journal.)

rather minor. The value of $T_e = 11376 \pm 1050$ K reported by Dicker et al. (2009) was based on data taken at 1.5 GHz and 21.5 GHz, but from Figure 4, data taken at frequencies larger than 1.5 GHz do not provide strong constraints on T_e values. In addition, the maximum intensities reported by Dicker et al. (2009) exceed those of Felli et al. (1993; 1.5 GHz) and Wilson & Pauls (1984; 23 GHz) by a factor of 1.3; we believe that this factor reflects an inconsistency in the value of the beam areas used to obtain the intensity units. For 1.5 GHz, there is excellent agreement between the integrated flux densities reported by Felli et al. (1993) and van der Werf & Goss (1989). However, the maximum value of integrated flux density at 1.5 GHz from the improved WJ model is 28% larger than these flux densities, so some more extended structure has not been recorded by the VLA. If the missing flux density is uniformly distributed over $30'$, the intensity is 22 mJy beam^{-1} or 0.2 MJy sr^{-1} , for a $28''$ resolution. For the model in Table 1, this additional intensity will have a negligible effect.

The shapes of the curves in Figures 1 and 3 are quite different from those of our Figure 4 or Figure 7 of Dicker et al. (2009). This is because the optical depths in NGC 1976 are significant at 330 MHz. In the improved WJ model, the sum of the optical depths, τ , of layers 7 and 8 is 1.9, while at frequencies higher than 1.5 GHz, the value of τ for these layers is <0.1 . The inclusion of the 330 MHz data is a crucial input for any test of the models of NGC 1976.

4. DISCUSSION

Early measurements of RRLs gave values of T_e that were markedly lower than values determined from collisionally excited lines of O^{++} in the optical (see, e.g., Goldberg 1966). In one response to these results, Peimbert (1967) pointed out that the collisionally excited lines (CELs) are biased toward high values of T_e while the RRLs are biased toward lower values. To compare these radio and optical data, Peimbert (1967) introduced an unbiased temperature, T_0 and a factor to

Table 1
An Improved Model of NGC 1976 from Radio Astronomy Data

Layer	T_e (K)	Line-of-sight Path ^a (pc)	N_e (cm^{-3})	Mean Diameter (pc)	Fraction of He ⁺	Turbulent Velocity ^b (km s^{-1})
1	8500	6.0 (−3)	1.2 (4)	0.08	1	10
2	8500	7.0 (−3)	1.0 (4)	0.17	1	10
3	8500	9.0 (−3)	8.9 (3)	0.25	1	15
4	8500	1.6 (−2)	7.5 (3)	0.34	1	15
5	8000	2.3 (−2)	5.4 (3)	0.42	1	15
6	8000	2.8 (−2)	3.7 (3)	0.59	1	15
7	7000	3.7 (−2)	2.7 (3)	0.76	0.75	12
8	7000	3.9 (−2)	1.7 (3)	1.10	0.75	12
9	6000	2.0 (−1)	3.0 (2)	1.85	0.5	12

Notes.

^a The values in parentheses are the powers of 10.

^b Three-dimensional non-thermal turbulent velocity.

characterize the fluctuations, t^2 . The value of T_0 is defined as

$$T_0(N_i, N_e) = \frac{\int T(r) N_i(r) N_e(r) d\Omega dl}{\int N_i(r) N_e(r) d\Omega dl}, \quad (2)$$

where T is the electron temperature, N_i is the ion density, and r is the distance along the line of sight. The integration is over the angular resolution. The fluctuation in T_0 is given by

$$t^2 = \frac{\int (T(r) - T_0)^2 N_i(r) N_e(r) d\Omega dl}{T_0^2 \int N_i(r) N_e(r) d\Omega dl}. \quad (3)$$

Using the improved WJ model (Table 1), there can be two extreme values of t^2 . The first is for a very small angle and the second for integration over the entire source. The values for the very small angle are $T_0 = 8250$ K and $t^2 = 3 \times 10^{-3}$. For the entire source these are $T_0 = 7600$ K and $t^2 = 10^{-2}$. The very small angle result is most relevant for comparisons with optical results. According to Peimbert (1967), the value of T_0 from RRLs, $T(\text{RRL})$, is weighted as

$$T(\text{RRL}) = T_0[1 - 1.42 t^2].$$

For the optical CELs such as the optical [O III] lines, the result is

$$T(\text{CEL}) = T_0 \left[1 + \frac{1}{2} \left(\frac{90800}{T_0} - 3 \right) t^2 \right].$$

For our value of t^2 , $T(\text{RRL}) = T(\text{CEL})$. Our values are $\sim 10\%$ of the values given by Esteban et al. (2004), who estimated that t^2 is between 0.02 and 0.03 with a favored best value of 0.022 ± 0.002 . This cannot be reconciled with our model, but indicates that structure on a finer scale than our $80''$ – $90''$ resolution is present. Higher values of T_e could arise in higher density clumps. Tsamis et al. (2008) have discussed effects that lead to finite t^2 values in planetary nebulae. The possibilities are fluctuations in T_e or in abundances of N or O. For NGC 1976, we find that if the t^2 values were due to physical variations in T_e rather than to abundance variations, then the fine angular scales sampled by the optical studies are dominated by compact T_e maxima, which are averaged in our coarser resolution (but see Tsamis et al. 2011).

Baldwin et al. (1991) report a value up to $T_e = 12,000$ K from measurements of singly ionized nitrogen, [N II]. The line ratios are more uncertain, but largest values of T_e from these lines are thought to arise in a small region near the exciting

star θ^1 C Orionis. Their measurements of the [O III] lines give T_e values in better agreement with radio data and our model. The RRL data for the densest region give lower values, with T_e ranging from 8300 K to 8600 K; these data were taken with $\sim 1'$ beams, so are averages over a larger region. O'Dell & Harris (2010) find a maximum value of $T_e = 8610 \pm 640$ K and review previous optical results. Other approaches to the question of element abundances and the value of T_e are possible. For example, Rubin et al. (1998) have used the *Hubble Space Telescope* (HST) to measure ultraviolet lines of [N II] and [O II]. By forcing agreement between abundance ratios from optical and UV measurements, they find $T_e = 9500$ K, $t^2 = 0.032$, and $N_e = 7 \times 10^3 \text{ cm}^{-3}$. From the large values of N_e , these lines must be associated with the model layers 1–4. The solution for T_e and N_e depends on combining measurements in the optical and UV data. It is possible that calibration errors may contribute to T_e values differing from our determination of T_e , since more recent data of O'Dell & Harris (2010) favor T_e values lower than 10^4 K throughout NGC 1976. The model in Table 1 must be considered the best representation of radio data, since this predicts a fall-off of T_e in the foreground region, layer 9, with the largest T_e values in the rear part of the H II region, as in the results of O'Dell & Harris (2010). The turbulent linewidths (last column of Table 1) represent the non-thermal motions. However, the data were taken with angular resolutions lower than for optical measurements. From the study of O'Dell et al. (2003), these non-thermal motions are found on even the finest angular scales.

Other than NGC 1976, only a few sources have been studied in infrared fine structure lines (see Afflerbach et al. 1997), but the source sample will be enlarged by Herschel Space Observatory and the start of science flights with the Stratospheric Observatory for Far-IR Astronomy (SOFIA). As a preparation for future surveys, detailed models of nearby sources are of value, especially from comparisons of different methods that allow the assessment of systematic effects.

5. CONCLUSIONS

The analysis of the intensities of pairs of high-resolution continuum images gives strong support to a small modification of the WJ model, which is based on RRL data. The WJ model is based on data averaged over $40''$ ($=0.08$ pc at 420 pc), so represents large-scale trends. In this model, there is a monotonic variation, from $T_e = 6000$ K to 8500 K. The lowest T_e arises from the most extended, lowest density foreground gas. The

highest T_e value arises from the densest, most compact region that is further from the Sun and abuts the molecular cloud; this is the location of the ionization front, so T_e and N_e monotonically decreases from the ionization front to the region of low density gas. The model gives a T_e fluctuation value, t^2 , which is $\sim 10\%$ of the values deduced from optical data. This is an indication that small-scale structure in T_e is averaged out by our lower angular resolution.

We thank W. M. Goss, R. Subrahmanyam, and G. Taylor for providing the digital form of the images used in the analysis. C. R. O'Dell and Y. Tsamis provided useful comments, as did an anonymous referee. The National Radio Astronomy Observatory is a facility of the National Science Foundation operated under cooperative agreement by Associated Universities, Inc. This research was performed while an author held a National Research Council Research Associateship Award at the US Naval Research Laboratory. S.C. acknowledges support from Millennium Science Initiative, Chilean Ministry of Economy: Nucleus P10-022-F, from FONDECYT grant 1100221, and from the CATA (“Fondo Basal PFB-06, CONICYT”).

APPENDIX

After the discovery of RRLs, it was assumed that these were emitted in local thermodynamic equilibrium (LTE). If so, the integrated line-to-continuum ratio allowed a direct estimate of the electron temperature, T_e . Under the assumption of LTE, the expression is

$$T_e^* = \frac{1.91 \times 10^4}{R \langle g_{\text{ff}}(T_e^*) \rangle} \left(\frac{N^+}{N_e} \right), \quad (\text{A1})$$

where T_e^* is the electron temperature in Kelvins, calculated under the assumption of LTE, R is the integrated line-to-continuum ratio in units of km s^{-1} , N^+ represents the number of ions, in this case H^+ , while N_e represents the total number of electrons from all ions, $\langle g_{\text{ff}}(T_e^*) \rangle$ is the Gaunt factor (Equation (A5)), and ν is the line frequency in GHz. This expression must be solved iteratively.

However, the formation of RRLs is a non-LTE process (see Goldberg 1966; Gordon & Sorochenko 2009). In the following, we restrict the discussion to hydrogen RRL emission in a source such as NGC 1976. The level populations are determined by the capture of free electrons into levels with high principal quantum numbers, n , followed by radiative decay to levels $n = 1$ or 2, followed by reionization. For high n levels, collisions play a larger role, while for low n levels, radiative decay is more important. The level populations for level n are described by the departure coefficients or b factors (ratios of the actual to the LTE population for a principal quantum number n). The value of b is a function of n , N_e , and T_e . As n approaches 1, b approaches zero monotonically. For the hydrogen atom, b is always less than unity. The b factor accounts for a lowering of energy level populations caused by radiative decay; for large n , b approaches unity. Another factor, β , is used to describe the difference in population between energy levels. The population of a higher level is larger than level n , so since $kT_e \gg h\nu$. This population difference leads to an amplification of the combined background consisting of continuum and spectral line emission. The amplification factor, β , depends on geometry, N_e and T_e ; b causes a reduction in line intensity while β causes an increase in line intensity. For $n > 100$, collisions shift line intensity to the line wings. For NGC 1976, from the models of Shaver (1980)

and WJ, at frequencies between 4 GHz ($n \sim 120$) and 30 GHz ($n \sim 60$) the effects of lower population and line amplification are rather small and largely compensate.

Non-LTE effects influence the intensity of RRLs. RRL emission is affected by (1) a lowering of the energy level population and thus the line intensity by the factor $b < 1$, (2) line masering which increases the line intensity, as expressed by the factor β , and (3) collisional broadening. In the formulation of BS, the relation between T_e and T_e^* is

$$T_e = b T_e^* \left(1 + \frac{1}{2} \beta \cdot \tau \right) \cdot \frac{\langle g_{\text{ff}}(T_e^*) \rangle}{\langle g_{\text{ff}}(T_e) \rangle}, \quad (\text{A2})$$

where τ is the optical depth in both line and continuum. Accurate values of b and β are needed to determine source parameters; see BS for sample values and applications to NGC 1976. Qualitatively, effect (2) is important if a low value of N_e is combined with large continuum intensity. Then this can lead to large amounts of RRL masering. Since large amounts of line masering are not found, the local density must be raised. In the case of NGC 1976, this was done by assuming that the emission arises from thin face-on slabs. This is consistent with the H II region located at the front side of a massive molecular cloud. Effect (3) is important for frequencies $\nu < 2$ GHz in NGC 1976. Then lines are broadened by collisions with free electrons, since these atoms have larger sizes. The larger linewidths may be inadvertently removed in baseline fits, so that some of the line emission may not be recorded. As noted by LB, the analysis of RRL data is made more reliable by plotting the line-to-continuum ratios and linewidths separately, rather than plotting the integrated line intensities.

For continuum measurements, the simplest expression is for a uniform temperature slab, as in Equation (1), where detailed physics is contained in τ_{ff} . This is given by the classical expression:

$$\tau_\nu = 3.014 \times 10^{-2} \left(\frac{T_e}{\text{K}} \right)^{-3/2} \left(\frac{\nu}{\text{GHz}} \right)^{-2} \left(\frac{\text{EM}}{\text{pc cm}^{-6}} \right) \langle g_{\text{ff}} \rangle \quad (\text{A3})$$

where EM is the emission measure of an ionized gas. If one neglects singly ionized helium, this becomes $N_i = N_e$:

$$\text{EM} = \int_0^s N_e^2 ds. \quad (\text{A4})$$

For an LOS depth “ s ” equal to the observed diameter, the density will be the rms value. For the NGC 1976 geometry, the RRL data were used to determine N_e and from this, the LOS depth must be much smaller than the diameter of a layer. And the classical expression for the Gaunt factor is that given by (Oster 1961):

$$\langle g_{\text{ff}} \rangle = \ln \left[4.955 \times 10^{-2} \left(\frac{\nu}{\text{GHz}} \right)^{-1} \right] + 1.5 \ln \left(\frac{T_e}{\text{K}} \right), \quad (\text{A5})$$

where “ $\langle \rangle$ ” signifies an average over velocities.

In the literature, one finds some other expressions for the Gaunt factor but these differ only by a constant factor. For example, Beckert et al. (2000) used a Gaunt factor that is 1.73 times larger than Equation (A5). Altenhoff et al. (1960) had approximated the Gaunt factor by a power-law relation in T_e and ν :

$$\tau_\nu = 8.235 \times 10^{-2} \left(\frac{T_e}{\text{K}} \right)^{-1.35} \left(\frac{\nu}{\text{GHz}} \right)^{-2.1} \left(\frac{\text{EM}}{\text{pc cm}^{-6}} \right) a(\nu, T_e). \quad (\text{A6})$$

with the correction $a(\nu, T)$ of ~ 1 . This expression for τ has been used for many calculations in the radio range. This is valid for $\nu < 10$ GHz, but there are significant deviations from the classical expression for $\langle g_{\text{ff}} \rangle$ at higher frequencies, even for T_e values of 7000 K (see Beckert et al. 2000). Thus, one should use the classical expression for τ_{ff} , that is, the combination of Equations (A3) and (A5), but *not* Equation (A6), to avoid errors for frequencies > 10 GHz. The exact calculation for the Gaunt factor for T_e values below 10^3 K must be calculated using the more accurate formulae, such as those summarized in Casassus et al. (2007).

For the transfer of continuum radiation through regions of differing T_e , one requires a more elaborate relation. For a ray through the center of NGC 1976, the WJ model listed in Table 1 gives

$$T_B = T_e(1) \cdot (1 - e^{-(\tau_1+\tau_2+\tau_3+\tau_4)}) \cdot e^{-(\tau_5+\tau_6+\tau_7+\tau_8+\tau_9)} \\ + T_e(5) \cdot (1 - e^{-(\tau_5+\tau_6)}) \cdot e^{-(\tau_7+\tau_8+\tau_9)} \\ + T_e(7) \cdot (1 - e^{-(\tau_7+\tau_8)}) \cdot e^{-\tau_9} + T_e(9) \cdot (1 - e^{-\tau_9}). \quad (\text{A7})$$

For the emission from layer 9 only, this reduces to Equation (1). For rays offset from the center, contributions from some layers may be absent since their lateral extents are different. Applying this relation to the original WJ model, for frequencies of 330 MHz and 1.5 GHz, gives the curve in Figure 1. The improved model, with parameters in Table 1 and a side view in Figure 2, results in the curve shown in Figure 3. For the frequencies 10.6 GHz and 1.5 GHz, this results in the curve shown in Figure 4.

REFERENCES

- Afflerbach, A., Churchwell, E., Accord, J. M., et al. 1996, *ApJS*, 106, 423
 Afflerbach, A., Churchwell, E., & Werner, M.W. 1997, *ApJ*, 478, 190
 Altenhoff, W. J., Mezger, P. G., Wendker, H., & Westerhout, G. 1960, *Veroeff. Sternwarte Bonn*, 59, 48
 Baldwin, J. A., Ferland, G. J., Martin, P. G., et al. 1991, *ApJ*, 374, 580
 Beckert, T., Duschl, W. J., & Mezger, P. G. 2000, *A&A*, 356, 1149
 Brocklehurst, M., & Seaton, M. J. 1972, *MNRAS*, 157, 179 (BS)
 Casassus, S., Nyman, L.-Å., Dickinson, C., & Pearson, T. J. 2007, *MNRAS*, 382, 1607
 Dicker, S., Mason, B. S., Korngut, P. M., et al. 2009, *ApJ*, 705, 226
 Esteban, C., Peimbert, M., Garcia-Rojas, J., et al. 2004, *MNRAS*, 355, 229
 Felli, M., Churchwell, E., Wilson, T. L., & Taylor, G. B. 1993, *A&AS*, 98, 137
 Goldberg, L. 1966, *ApJ*, 144, 344
 Gordon, M. A., & Sorochenko, R. L. 2009, *Radio Recombination Lines* (Berlin: Springer)
 Hirota, T., Bushimata, T., Choi, Y. K., et al. 2007, *PASJ*, 59, 897
 Lockman, F. J., & Brown, R. L. 1975, *ApJ*, 201, 134 (LB)
 Menten, K. M., Reid, M. J., Forbrich, J., & Brunthaler, A. 2007, *A&A*, 474, 515
 Mills, B. Y., & Shaver, P. A. 1968, *Aust. J. Phys.*, 21, 95
 O'Dell, C. R. 2001, *ARA&A*, 39, 99
 O'Dell, C. R. 2003, *The Orion Nebula, Where Stars are Born* (Cambridge, MA: Harvard Univ. Press)
 O'Dell, C. R., & Harris, J. A. 2010, *AJ*, 140, 985
 O'Dell, C. R., Peimbert, M., & Peimbert, A. 2003, *AJ*, 125, 2590
 Oster, L. 1961, *Rev. Mod. Phys.*, 33, 525
 Peimbert, M. 1967, *ApJ*, 150, 825
 Rodriguez-Franco, A., Wilson, T. L., Martin-Pintado, J., & Fuente, A. 2001, *ApJ*, 559, 985
 Rubin, R. H., Martin, P. G., Dufour, R. J., et al. 1998, *ApJ*, 495, 891
 Sandstrom, K., Peek, J. E. G., Bower, G., Bolatto, A. D., & Plambeck, R. L. 2007, *ApJ*, 667, 1161
 Shaver, P. A. 1980, *A&A*, 90, 34
 Subrahmanyam, R., Goss, W. M., & Malin, D. M. 2001, *AJ*, 121, 399
 Terzian, Y., & Parrish, A. 1970, *Astrophys. Lett.*, 5, 261
 Tsamis, Y. G., Walsh, J. R., Pequignot, D., et al. 2008, *MNRAS*, 386, 22
 Tsamis, Y. G., Walsh, J. R., Vilchez, J. M., & Pequignot, D. 2011, *MNRAS*, 412, 1367
 van der Werf, P. P., & Goss, W. M. 1989, *A&A*, 224, 209
 Wilson, T. L., Filges, L., Codella, C., Reich, W., & Reich, P. 1997, *A&A*, 327, 1177
 Wilson, T. L., & Jaeger, B. 1987, *A&A*, 184, 291 (WJ)
 Wilson, T. L., & Pauls, T. A. 1984, *A&A*, 138, 225
 Wilson, T. L., Rohlf, K., & Huettmeister, S. 2009, *Tools of Radio Astronomy* (5th ed.; Berlin: Springer)